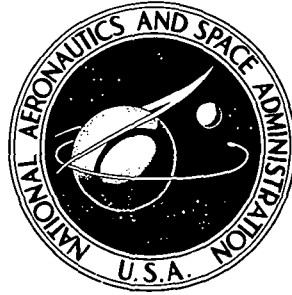


N74-10325

NASA TECHNICAL NOTE



NASA TN D-7486

NASA TN D-7486

**CASE FILE
COPY**

**EXPERIMENTAL AND ANALYTICAL STUDY
OF A CONICALLY DIFFUSED FLOW WITH
A NEARLY SEPARATED BOUNDARY LAYER**

by Donald R. Boldman and Harvey E. Neumann

Lewis Research Center

Cleveland, Ohio 44135

NATIONAL AERONAUTICS AND SPACE ADMINISTRATION • WASHINGTON, D. C. • NOVEMBER 1973

1. Report No. NASA TN D-7486	2. Government Accession No.	3. Recipient's Catalog No.	
4. Title and Subtitle EXPERIMENTAL AND ANALYTICAL STUDY OF A CONICALLY DIFFUSED FLOW WITH A NEARLY SEPARATED BOUNDARY LAYER		5. Report Date November 1973	
		6. Performing Organization Code	
7. Author(s) Donald R. Boldman and Harvey E. Neumann		8. Performing Organization Report No. E-7423	
		10. Work Unit No. 501-24	
9. Performing Organization Name and Address Lewis Research Center National Aeronautics and Space Administration Cleveland, Ohio 44135		11. Contract or Grant No.	
		13. Type of Report and Period Covered Technical Note	
12. Sponsoring Agency Name and Address National Aeronautics and Space Administration Washington, D. C. 20546		14. Sponsoring Agency Code	
		15. Supplementary Notes	
16. Abstract <p>Turbulence measurements were obtained in the nearly separated flow in a 13^o total angle of divergence conical diffuser coupled to a constant area tailpipe. Air at 207 newtons per square centimeter and 308 K provided an inlet velocity of about 51 meters per second at an inlet unit Reynolds number of 63.7×10⁶ per meter. Very high longitudinal turbulence intensities accompanied the diffusion process with peak values approaching 40 percent when normalized by the local centerline velocity. Predictions of the pressure recovery coefficient using a mixing length concept were good in the early stages of diffusion. In the latter stages of diffusion satisfactory predictions of the pressure recovery were obtained with an empirical method.</p>			
17. Key Words (Suggested by Author(s)) Boundary layer Separation Turbulence Diffuser		18. Distribution Statement Unclassified - unlimited	
19. Security Classif. (of this report) Unclassified	20. Security Classif. (of this page) Unclassified	21. No. of Pages 40	22. Price* Domestic, \$3.00 Foreign, \$5.50

* For sale by the National Technical Information Service, Springfield, Virginia 22151

EXPERIMENTAL AND ANALYTICAL STUDY OF A CONICALLY DIFFUSED FLOW WITH A NEARLY SEPARATED BOUNDARY LAYER

by Donald R. Boldman and Harvey E. Neumann

Lewis Research Center

SUMMARY

Turbulence measurements were obtained in the nearly separated flow in a 13° total angle of divergence conical diffuser coupled to a constant area tailpipe. Air at 207 newtons per square centimeter and 308 K provided an inlet velocity of about 51 meters per second at an inlet unit Reynolds number of 63.7×10^6 per meter. Very high longitudinal turbulence intensities accompanied the diffusion process with peak values approaching 40 percent when normalized by the local centerline velocity.

Comparison of the turbulence transport in the nearly separated boundary layer with values for flows with zero acceleration revealed that the ratio of turbulent shear to the turbulent kinetic energy was only about one-third of the value for boundary layers in zero acceleration. Also the peak values in the turbulent shear production and Reynolds stress generation terms were displaced further away from the wall in the case of the nearly separated boundary layer.

Predictions of the pressure recovery coefficient using a mixing length concept were good in the early stages of diffusion. Satisfactory predictions of the pressure recovery after predicted separation were obtained with an empirical constant effectiveness criterion. The best agreement was within 12 percent of the experimental pressure recovery.

INTRODUCTION

A knowledge of the turbulent transport associated with the subsonic diffusion of air is important in the design of components for high performance aircraft. With subsonic diffusion, a rise in static pressure is obtained at the expense of a reduction in momentum. Eventually the flow in the decelerated boundary layer near the wall has insufficient momentum to accommodate the increase in pressure and the flow will tend to separate.

During separation, viscous losses are high and consequently, the diffusion process becomes very inefficient. In most practical diffusers, it is desirable to avoid separation; however, it is often necessary to operate the diffuser in a state of partial or incipient separation. The present study was performed in an effort to learn more about the turbulent structure of a diffusing flow which is in this state of incipient separation.

In the present study a diffuser calculation method (ref. 1) based on the mixing length concept was applied to the flow in a conical diffuser having a nearly separated boundary layer. The predicted mean velocity profiles and pressure recovery are compared to the experimental results using a standard two-layer turbulence model. Results are also presented for a modified outer region turbulence model which was suggested on the basis of turbulence measurements in the diffuser. The constant effectiveness criterion of reference 2 is used to extend the pressure recovery prediction after separation.

All of the present tests were conducted using a 13° total angle of divergence diffuser coupled to a constant area tailpipe. The working fluid consisted of air at a nominal pressure of 207 newtons per square centimeter and a nominal total temperature of 308 K. A critical flow nozzle at the exit of the tailpipe was used to limit the inlet velocity to about 51 meters per second (inlet unit Reynolds number of $63.7 \times 10^6/m$) in order to stay within the incompressible flow regime. Hot-wire anemometers were used to measure the mean velocity profiles, longitudinal and lateral components of turbulence intensity, and the Reynolds stress.

SYMBOLS

A	area
a	constant in hot-wire calibration equation
a_1	constant in hot-wire calibration equation
b	constant in hot-wire calibration equation
b_1	constant in hot-wire calibration equation
C_f	skin friction coefficient
C_p	pressure recovery coefficient
D	diameter
E	bridge voltage
e	fluctuating component of voltage
K	constant in equation for the mixing length (eq. (7))

K_1	constant in outer region turbulence model (eq. (9))
K_2	term in equation for mixing length (eqs. (7) and (8))
l	mixing length
M	Mach number
n	mass flux exponent in hot-wire calibration equation
P	pressure
q	turbulence kinetic energy function, $\overline{q^2} = \overline{u^2} + \overline{v^2} + \overline{w^2}$
R	radius
Re	Reynolds number
T	temperature
U	mean longitudinal velocity
u	longitudinal fluctuating component of velocity
u'	root-mean-square (rms) value of u
V	effective velocity sensed by hot wire
v	lateral fluctuating component of velocity
v'	root-mean-square (rms) value of v
w	fluctuating component of velocity normal to x-y plane
w'	root-mean-square (rms) value of fluctuating component of velocity normal to u and v components
X	defined by eq. (B10)
x	axial direction
Y	defined by eq. (B11)
y	distance from wall along normal
α	angle between wire number I of X-wire probe and mean flow direction
β	angle between wire number II of X-wire probe and mean flow direction
γ	ratio of specific heats
δ	boundary layer thickness
δ^*	boundary layer displacement thickness
ϵ	eddy viscosity

η	pressure recovery effectiveness, $C_p / (C_{p, id})_i$
μ	dynamic viscosity
ν	kinematic viscosity
ρ	density
σ	local half angle of divergence of diffuser
θ	boundary layer momentum thickness
τ	shear stress
φ	angle between wires of X-wire probe and mean flow direction

Subscripts:

c	compressible or centerline value
e	ambient conditions
i	incompressible
id	ideal
in	inner region of boundary layer
l	laminar
o	diffuser entrance
out	outer region of boundary layer
ref	reference value
sep	condition at separation
t	turbulent
w	condition associated with hot wire or wall
θ	based on momentum thickness
0	stagnation condition

Superscript:

—	average value
---	---------------

APPARATUS

The geometry, surface finish, and operating conditions for the present study were selected largely on the basis of the empirical design criteria of reference 3. In an

effort to obtain a nearly separated diffusing flow, a conical diffuser having a 13° total angle of divergence was chosen for this experiment. The diffuser was coupled to constant diameter pipe sections both upstream and downstream of the diffuser as shown in figure 1. The wall radii of curvature at the diffuser entrance and exit were equal to the entrance diameter D_0 , where $D_0 = 7.62$ centimeters. The inlet, diffuser, and tailpipe were fabricated from AISI 304 stainless steel and were machined to a relatively smooth internal surface finish of 81.2 microcentimeters rms.

Air entered the diffuser through a plenum, bellmouth, and 7.62-centimeter-diameter by 27.3-centimeter-long pipe inlet as shown in figure 1. A 3.81-centimeter-diameter critical flow nozzle was located downstream of the tailpipe. Coordinates for the diffuser and tailpipe sections are given in table I.

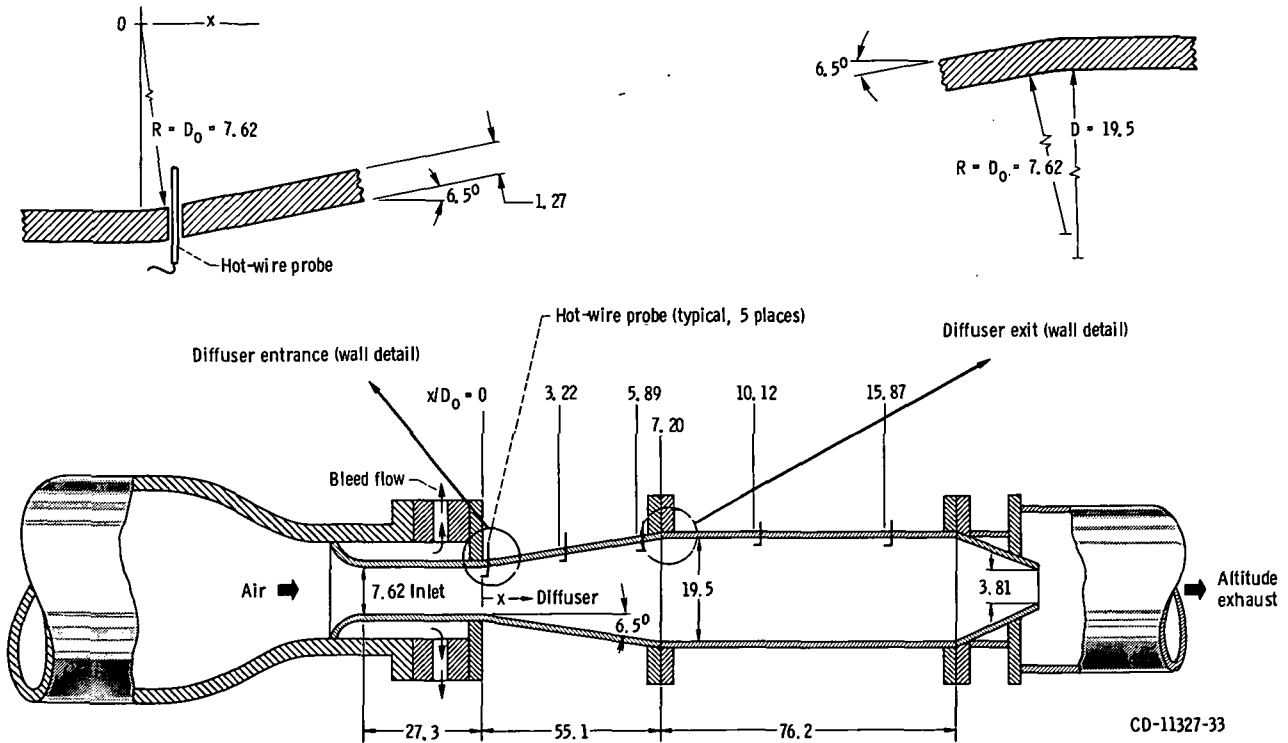


Figure 1. - Apparatus for study of diffusing flow. Inlet diameter, $D_0 = 7.62$ centimeters. (All dimensions in cm).

TABLE I. - DIFFUSER AND TAILPIPE
COORDINATES

[Inlet diameter, $D_0 = 7.62$ cm; inlet area,
 $A_0 = 45.6 \text{ cm}^2$]

Station	Axial distance, x, cm	Diameter, D, cm	Axial distance, x/D ₀	Area ratio, A/A ₀
^a 0	0	7.620	0	1.000
1	4.209	8.458	.553	1.232
2	6.749	9.032	.886	1.405
3	9.296	9.614	1.220	1.592
4	11.829	10.191	1.553	1.789
5	14.369	10.767	1.886	1.997
6	16.911	11.346	2.220	2.217
7	19.451	11.923	2.553	2.448
8	21.989	12.497	2.886	2.690
^a 9	24.524	13.071	3.219	2.942
10	27.069	13.653	3.553	3.210
11	29.609	14.229	3.886	3.487
12	32.151	14.803	4.220	3.774
13	34.686	15.380	4.552	4.074
14	37.229	15.956	4.886	4.385
15	39.769	16.528	5.219	4.705
16	42.314	17.104	5.553	5.039
^a 17	44.869	17.686	5.889	5.387
(b)	54.864	19.533	7.200	6.571
18	62.484	↓	8.200	↓
^a 19	77.089	↓	10.117	↓
20	91.694	↓	12.034	↓
21	106.299	↓	13.950	↓
^a 22	120.904	↓	15.867	↓

^aDenotes boundary layer survey station.

^bTangency.

INSTRUMENTATION

Wall Static Pressures

Pressure taps having a diameter of 0.0794 centimeter were located in the diffuser and tailpipe starting at the diffuser entrance ($x/D_0 = 0$ in fig. 1). A pressure tap was located at each of the twenty-three stations listed in table I.

The static pressures were measured by means of manometers containing acetylene tetrabromide which has a nominal room temperature density of 2.934 grams per cubic centimeter. The stagnation pressure, measured at the plenum centerline, provided the reference pressure for the manometer system.

Boundary Layer Surveys

Hot-wire measurements of mean velocity, longitudinal and lateral components of turbulence intensity, and Reynolds stress were obtained at stations 9 and 17 in the diffuser and at stations 19 and 22 in the tailpipe (refer to table I). A single wire probe was used for the measurements of mean velocity and longitudinal components of turbulence intensity, whereas an X-wire probe was used to measure the lateral components of turbulence intensity and the Reynolds stress. Since the boundary layer at the diffuser entrance was too thin to accommodate the X-wire probe, only the mean velocity and longitudinal turbulence intensity distributions were measured at this location.

All of the hot-wire measurements were obtained with constant temperature hot-wire anemometers using 0.0005-centimeter-diameter tungsten hot wires. The hot-wire probes were moved point-by-point from the centerline to the wall by motorized actuators. The single wire probes were driven until contact with the wall was established. The X-wire probe traverse was terminated prior to contact with the wall by means of a sleeve located on the probe shaft. The minimum distance from the wire crossing point to the wall was 0.381 centimeter. Further details concerning the actuators and single wire probe design can be obtained from reference 4.

A pitot pressure probe having a flattened tip 0.005 centimeter high by 0.076 centimeter wide was also used to measure the velocity profile at $x/D_0 = 3.22$ in the diffuser. Details concerning the pressure probe design can be obtained from reference 5.

EXPERIMENTAL FLOW CONDITIONS

All data were obtained with the same nominal flow conditions. The stagnation pressure P_0 was maintained at 207 ± 1 newtons per square centimeter absolute. The stagnation temperature T_0 for the tests was 308 ± 3 K. These stagnation conditions provided a nominal inlet velocity U_0 of 51.3 meters per second and an inlet Reynolds number based on D_0 of 4.85×10^6 .

EXPERIMENTAL RESULTS

Pressure Recovery

The experimental pressure recovery in the diffuser and tailpipe is usually presented in terms of the pressure recovery coefficient C_p where

$$C_p = \frac{\left[\frac{P_w}{P_0} - \left(\frac{P_w}{P_0} \right)_0 \right] P_0}{\frac{1}{2} \rho \bar{U}_0^2} \quad (1)$$

The velocity \bar{U}_0 is the mass-averaged value at the diffuser inlet. The experimental values of C_p are often compared to the maximum attainable values for a one-dimensional flow of a perfect gas in a diffuser of the same geometry. These ideal values of C_p can be expressed as

$$(C_{p, id})_i = 1 - \frac{1}{\left(\frac{A}{A_0} \right)^2} \quad (2)$$

for incompressible flow and as

$$(C_{p, id})_c = \frac{\left(1 + \frac{\gamma - 1}{2} M^2 \right)^{-\gamma/(\gamma-1)} - \left(1 + \frac{\gamma - 1}{2} M_0^2 \right)^{-\gamma/(\gamma-1)}}{\frac{\gamma}{2} M_0^2 \left(1 + \frac{\gamma - 1}{2} M_0^2 \right)^{-\gamma/(\gamma-1)}} \quad (3)$$

for compressible flow. The experimental and ideal distributions of pressure recovery coefficient for the diffuser and tailpipe are presented in figure 2 and are tabulated in table II. The distributions of ideal pressure recovery, $(C_{p, id})_i$ and $(C_{p, id})_c$, in figure 2 indicate that the flow in this investigation can, for all practical purposes, be considered as incompressible. A maximum ideal pressure recovery coefficient of 0.977 is obtained at the diffuser exit and remains constant in the tailpipe (refer to eq. (2)). The experimental pressure recovery coefficients are appreciably lower than the ideal values

with $C_p = 0.72$ at the diffuser exit ($x/D_0 = 7.2$). The tailpipe provided only a modest increase in C_p of from 0.72 at the diffuser exit to about 0.75 near the tailpipe exit.

It is recognized that in the entrance region of the diffuser there is a modest favorable pressure gradient which can influence the value of $(P_w/P_0)_0$ used as the reference pressure in the pressure recovery coefficient (eq. (1)). An indication of the magnitude of this favorable pressure gradient in the present diffuser will be given in a later section entitled PREDICTED RESULTS.

The solid symbols in figure 2 represent the values of C_p at the boundary layer survey stations. It should be noted that a boundary layer survey was obtained at the diffuser entrance in the plane of the static pressure tap which was used for the reference pressure in computing C_p . The mean velocity profile at this station provided one of the input matching conditions for the diffuser flow analysis of reference 1.

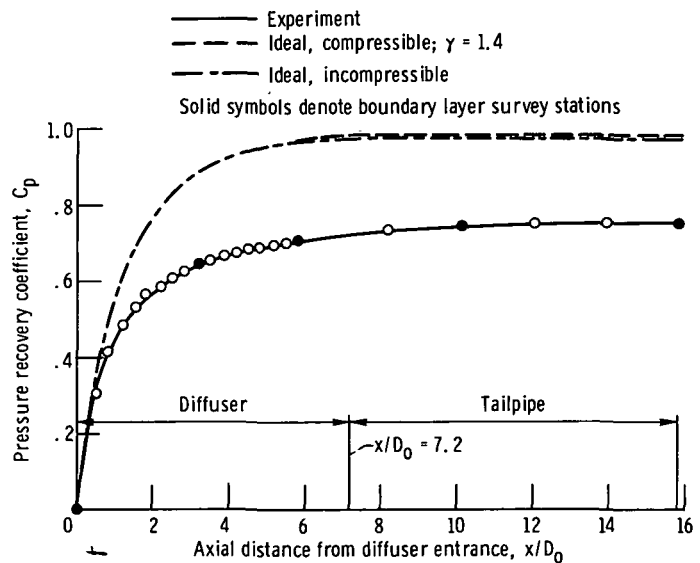


Figure 2. - Pressure distribution in diffuser and tailpipe. Inlet Reynolds number, $Re_0 \approx 63.7 \times 10^6$ per meter; inlet diameter, $D_0 = 7.62$ centimeters.

TABLE II. - EXPERIMENTAL AND IDEAL PRESSURE RECOVERY COEFFICIENTS

[Inlet diameter, $D_0 = 7.62$ cm; stagnation pressure, $P_0 = 207$ N/cm²]

Station	Axial distance, x/D_0	Pressure ratio, P_w/P_0	Mach number, M	Pressure recovery coefficient		
				Experimental C_p	Ideal incompressible C_{p, id_i}	Ideal incompressible C_{p, id_c}
^a 0	0	0.98528	0.146	0	0	0
1	.553	.98985	.121	.304	.341	.347
2	.886	.99152	.110	.416	.493	.500
3	1.220	.99253	.104	.484	.605	.613
4	1.553	.99323	.0986	.531	.687	.695
5	1.886	.99374	.0948	.566	.749	.756
6	2.220	.99406	.0923	.589	.797	.804
7	2.553	.99440	.0896	.611	.833	.840
8	2.886	.99464	.0877	.627	.862	.868
^a 9	3.219	.99487	.0858	.643	.885	.891
10	3.553	.99503	.0844	.654	.903	.909
11	3.886	.99529	.0833	.663	.918	.924
12	4.220	.99529	.0822	.672	.930	.936
13	4.552	.99542	.0810	.680	.940	.946
14	4.886	.99554	.0799	.689	.948	.954
15	5.219	.99561	.0793	.693	.955	.961
16	5.553	.99568	.0787	.698	.961	.966
^a 17	5.889	.99577	.0778	.704	.966	.971
18	8.200	.99617	.0741	.731	.977	.983
^a 19	10.117	.99637	.0721	.745	↓	↓
20	12.034	.99646	.0712	.751		
21	13.950	.99651	.0708	.754		
^a 22	15.867	.99651	.0708	.754	↓	↓

^aDenotes boundary layer survey station.

Boundary Layer Surveys

In this section, the results of hot-wire surveys of the mean velocity U , longitudinal component of turbulence intensity u' , lateral component of turbulence intensity v' , and the Reynolds stress \overline{uv} will be presented. The turbulence measurements were obtained with single and X-wire probes. A linearized circuit was used in conjunction with the single wire measurements to obtain the mean velocity profiles. Details concerning the hot-wire data reduction are presented in appendix A. As in the diffuser experiment of reference 6, the accuracy of the turbulence measurements was difficult to establish. In reference 6, the estimated errors which were based on the results of reference 7 were 5 percent in u' and 10 to 15 percent in \overline{uv} during the early stages of diffusion. In the latter stages of diffusion the estimated error increased to about 20 percent in u' and 20 to 40 percent in \overline{uv} . The latter stage of the diffusion process in the conical diffuser of this study probably occurs downstream of station 9 ($x/D_0 = 3.22$). The boundary layer data will be presented graphically but will not be tabulated because of the difficulty in determining the measurement error and the possibility of establishing a false sense of the measurement accuracy.

Another source of error in the turbulence measurements arises because of misalignment of the X-wire probe which results in unequal angles between the wires and the mean flow velocity vector. This error is present at station 9 ($x/D_0 = 3.22$) and at station 17 ($x/D_0 = 5.89$) in the diffuser because the probe is installed in a position normal to the wall. The effect of this misalignment error is to reduce the measured values of v' and \overline{uv} with the maximum reduction occurring at the centerline. The effects of this misalignment error will be ignored in the presentation of the turbulence data; however, the magnitude of the required correction at the centerline of stations 9 and 17 has been estimated in appendix B.

Before examining the profiles of mean velocity and turbulence intensity, consider the flow development in the diffuser and tailpipe in a qualitative manner. The flow in the present system is depicted schematically in figure 3. Actually, this figure is based on the profile data yet to be presented. The large inviscid core in the entrance region ($x/D_0 = 0$) rapidly becomes displaced by a turbulent core. The complete disappearance of the inviscid core takes place in the region bounded by $3.22 < x/D_0 < 5.89$ - probably just slightly downstream of $x/D_0 = 3.22$. In analyzing the results, emphasis will be placed on the data at $x/D_0 = 3.22$ since this station is the first one to reflect the effects of the strong adverse gradient in the entrance region.

Velocity profiles. - The boundary layer velocity profiles at the three stations in the diffuser and at the two stations in the tailpipe are presented in figure 4. The boundary layer velocity U is nondimensionalized by the local centerline value $U_c(x)$ which is

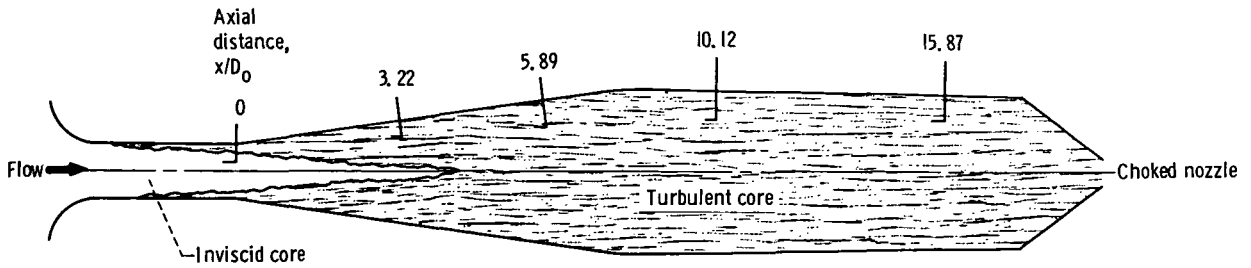


Figure 3. - Schematic of flow in diffuser and tailpipe (based on measured results). Inlet diameter, $D_0 = 7.62$ centimeters.

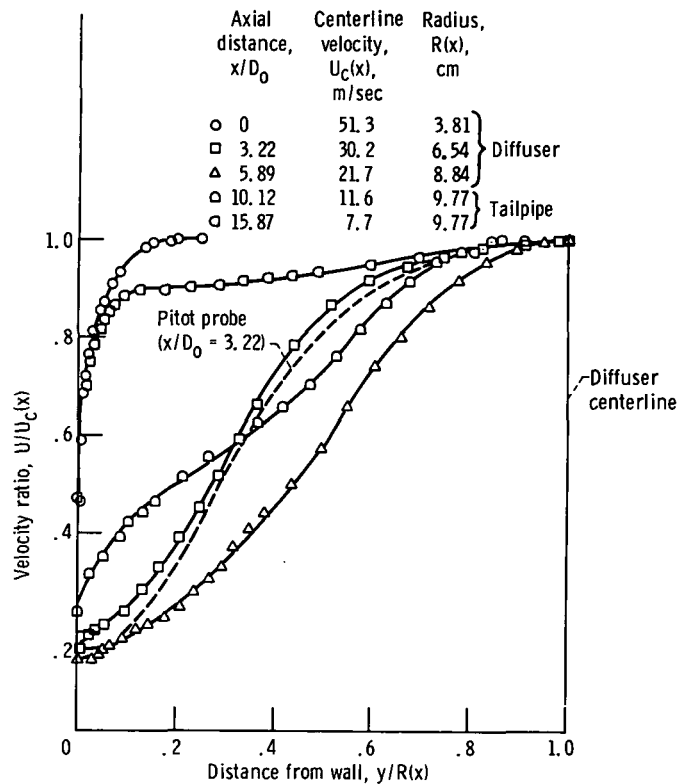


Figure 4. - Mean velocity profiles in diffuser and tailpipe. Inlet Reynolds number, $Re_0 \approx 63.7 \times 10^6$ per meter; inlet diameter, $D_0 = 7.62$ centimeters.

also the maximum velocity at a given station. The value of $U_c(x)$ decreases from 51.3 meters per second at the entrance to 7.7 meters per second at the downstream station in the tailpipe. The local radius $R(x)$, which is used to nondimensionalize the distance variable y , increases from 3.81 centimeters at the entrance to a maximum of 9.77 centimeters in the tailpipe.

Referring to figure 4, it can be noted that the boundary layer at the diffuser entrance is relatively thin, $\delta \approx 0.2 R(x)$; however, as the flow diffuses the boundary layer rapidly fills the channel. This rapid growth can be noted by comparing the profiles at $x/D_0 = 0$ and 3.22. The profiles at $x/D_0 = 3.22$ and 5.89 suggest that the boundary layer is in a nearly separated state. As in reference 8, the velocity near the wall approaches a value of about 20 percent of the local maximum $U_c(x)$. Furthermore the boundary layer profile near the wall is similar to the classical incipiently separated shape, that is, $\partial U/\partial y \rightarrow 0$. Further development of the viscous flow in the tailpipe results in a readjustment or relaxation to a nearly uniform profile across the duct ($x/D_0 = 15.87$).

A pitot pressure probe was also used to survey the velocities at $x/D_0 = 3.22$. Although the shape of the profile is different very close to the wall ($y/R(x) < 0.05$), the pitot probe results are generally in agreement with the hot-wire measurements and indicate the presence of incipient separation rather than actual separation.

Longitudinal component of turbulence intensity. - Radial distributions of the longitudinal component of turbulence intensity u' are represented in two different nondimensional forms, $u'/U_c(x)$ and u'/U_0 , and are presented in figures 5 and 6, respectively.

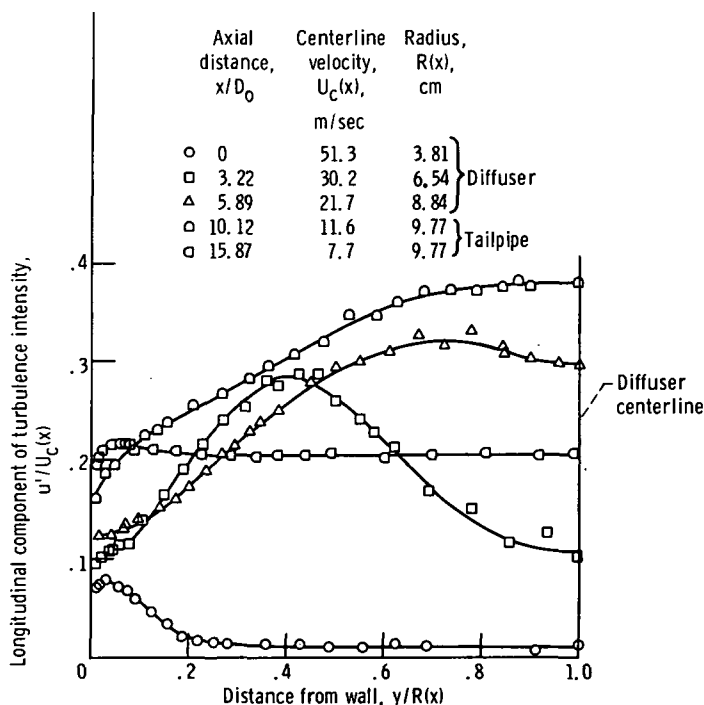


Figure 5. - Distributions of longitudinal component of turbulence intensity (normalized by local centerline velocity) in diffuser and tailpipe. Inlet Reynolds number, $Re_0 \approx 63.7 \times 10^6$ per meter; inlet diameter, $D_0 = 7.62$ centimeters.

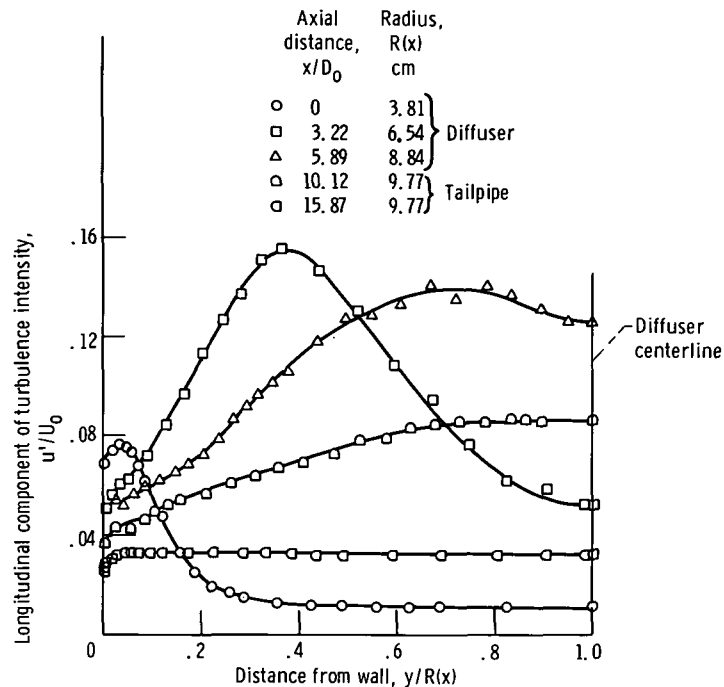


Figure 6. - Distributions of longitudinal component of turbulence intensity (normalized by entrance velocity) in diffuser and tailpipe. Inlet Reynolds number, $Re_0 \approx 63.7 \times 10^6$ per meter; inlet diameter, $D_0 = 7.62$ centimeters; inlet velocity, $U_0 = 51.3$ meters per second.

The nondimensionalization by U_0 provides a representation of the change in the absolute value of u' since U_0 , the diffuser entrance velocity, is a constant whereas the nondimensionalization by $U_c(x)$ gives an indication of the radial change in u' relative to the local centerline velocity. The same nondimensionalization will also be used in presenting the results of the lateral components of turbulence intensity v' and the Reynolds stress \overline{uv} .

The radial distributions of the longitudinal component turbulence intensity $u'/U_c(x)$ at the five stations are shown in figure 5. The profile at the diffuser entrance indicates a free stream intensity of about 1.0 percent and a maximum near the wall of about 8.0 percent. As the flow diffuses, the intensity increases appreciably with peak values of $u'/U_c(x)$ approaching 40 percent ($x/D_0 = 10.12$). The maximum in the intensity distribution moves toward the centerline as the flow diffuses. Near the exit of the tailpipe where the flow appears to be reestablishing some form of equilibrium, the maximum value of $u'/U_c(x)$ occurs near the wall. This trend of increasing turbulence intensity with decreasing axial velocity has also been observed by Spangenberg, Rowland, and Mease (ref. 9) in a two-dimensional diffusing flow near separation. In reference 9, values of u'/U in excess of 0.5 were obtained in a region very near the wall. Similar levels of u'/U occur in the wall region of the present diffuser at $x/D_0 = 3.22$. However, during the latter stages of diffusion, that is, at $x/D_0 = 5.89$ and 10.12 , these

high levels of intensity ($u'/U > 0.4$) extend from the wall region to approximately the duct centerline. This can be noted by dividing the intensity $u'/U_c(x)$ in figure 5 by the corresponding velocity ratio $U/U_c(x)$ in figure 4.

The distribution of u'/U_0 in figure 6 indicate that the absolute value of u' also increases as the flow passes from the entrance to the diffuser exit ($x/D_0 = 5.88$). The measurements indicate that the maximum value of u' is about 16 percent of the entrance velocity or about a factor of two higher than the observed maximum in u' at the diffuser entrance. This change in u'/U_0 is much less than the change in $u'/U_c(x)$ (fig. 5), thus indicating that a large part of the apparent increase in the intensity $u'/U_c(x)$ is the result of nondimensionalization by the local centerline velocity. A similar effect involving the method of nondimensionalizing u' has been observed in the boundary layer of accelerating flows (e.g., ref. 10).

Lateral component of turbulence intensity. - The radial distributions of the lateral component of turbulence intensity v' are presented in the two nondimensional forms in figures 7 and 8. Comparison of these results with the corresponding values of u' in

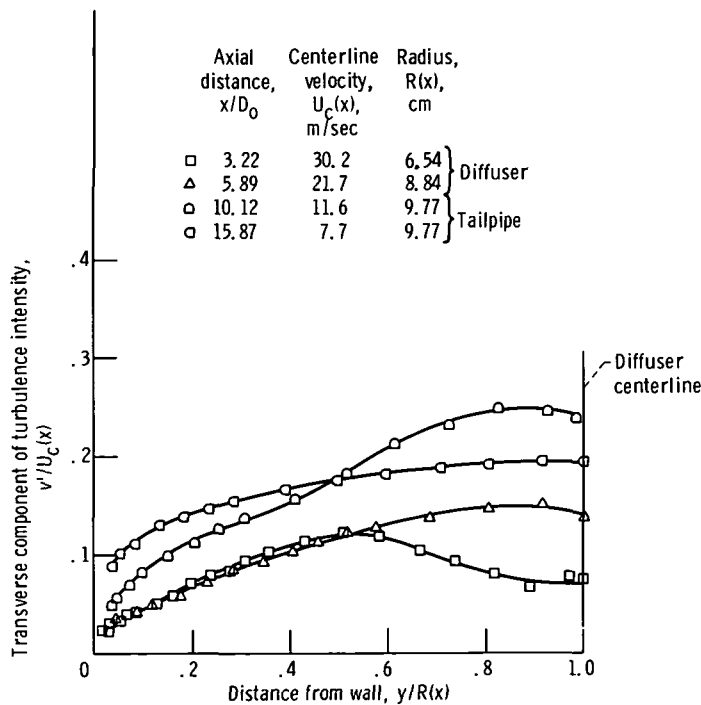


Figure 7. - Distributions of transverse component of turbulence intensity (normalized by local centerline velocity) in diffuser and tailpipe. Inlet Reynolds number, $Re_0 \approx 63.7 \times 10^6$ per meter; inlet diameter, $D_0 = 7.62$ centimeters.

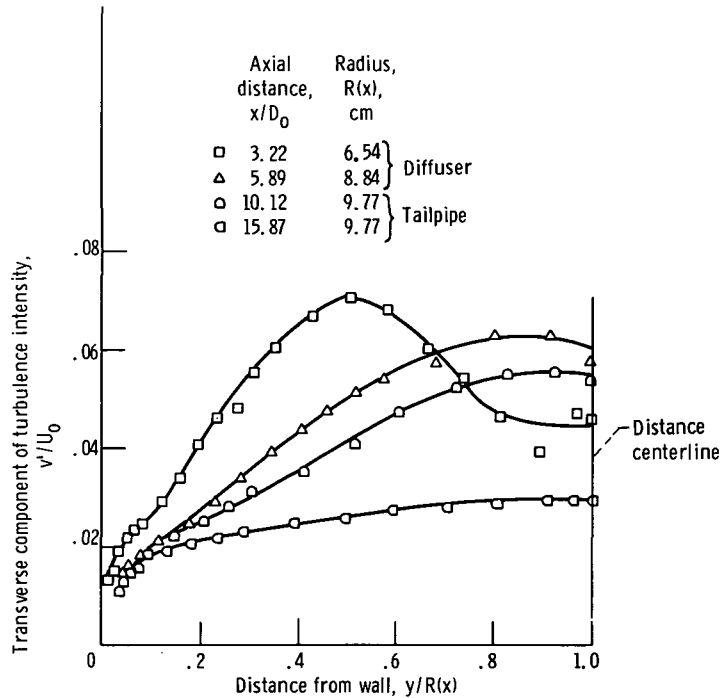


Figure 8. - Distributions of transverse component of turbulence intensity (normalized by entrance velocity) in diffuser and tailpipe. Inlet Reynolds number, $Re_0 \approx 63.7 \times 10^6$ per meter; inlet diameter, $D_0 = 7.62$ centimeters; inlet velocity, $U_0 = 51.3$ meters per second.

figures 5 and 6 indicates that v' is much less than u' . In the latter stages of diffusion, the maximum in v' moves towards the centerline. The maximum values of u' and v' at a given station occurred at about the same radial position.

Reynolds stress distributions. - The distributions of the Reynolds or shear stress functions $\overline{uv}/U_c(x)^2$ and \overline{uv}/U_0^2 are presented in figures 9 and 10, respectively. A maximum value of $\overline{uv}/U_c(x)^2$ of about 0.0085 occurs at $x/D_0 = 10.12$ (fig. 9) whereas the maximum in the absolute value of \overline{uv} occurs at $x/D_0 = 3.22$ as shown in figure 10. These values of \overline{uv} must be adjusted, however, for the errors mentioned previously and discussed in appendix B. In the next section the distribution of \overline{uv} at $x/D_0 = 3.22$ will be used in conjunction with the corresponding mean velocity profile to estimate the constant in the outer region of the Clauser (ref. 11) eddy viscosity model used in the analysis of reference 1.

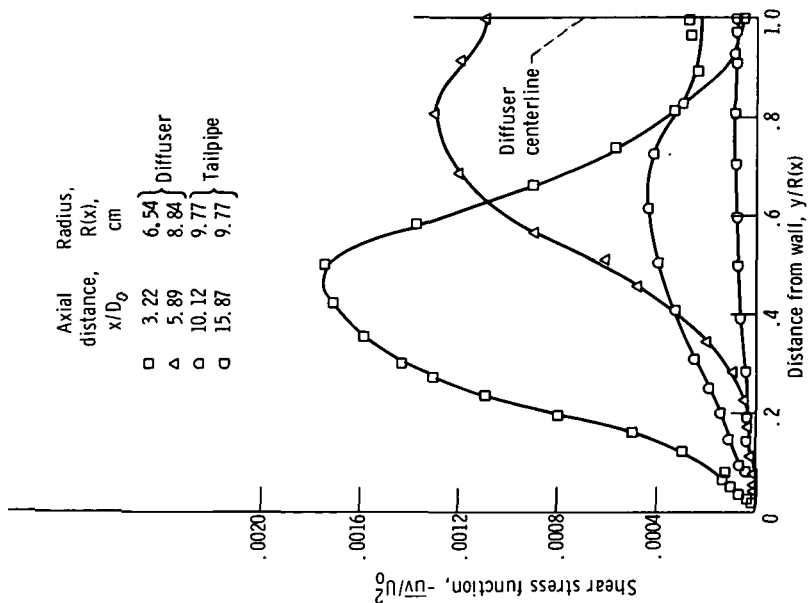


Figure 10. - Measurements of shear stress function (normalized by entrance velocity) in diffuser and tailpipe. Inlet Reynolds number, $Re_0 \approx 63.7 \times 10^6$ per meter; inlet diameter, $D_0 = 7.62$ centimeters; inlet velocity, $U_0 = 51.3$ meters per second.

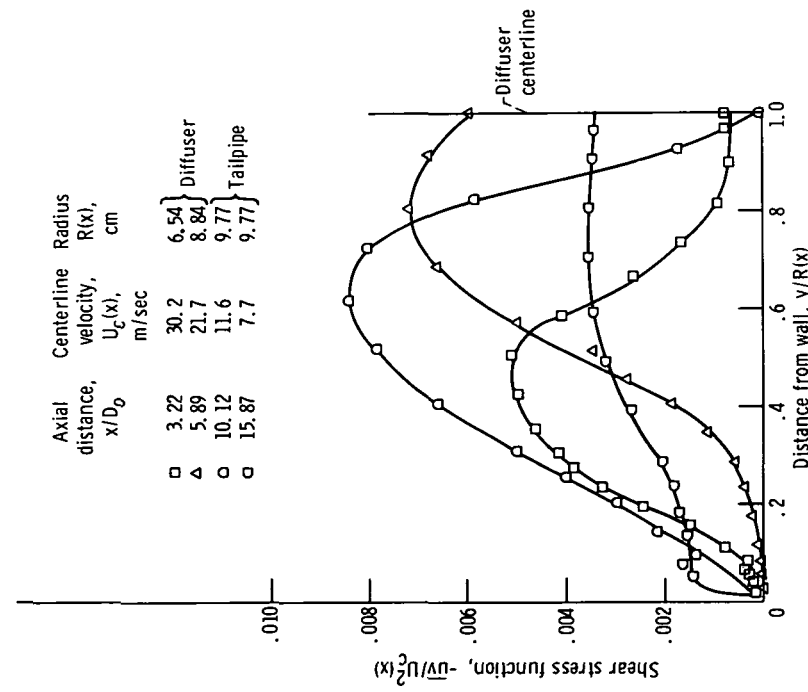


Figure 9. - Measurements of shear stress function (normalized by local centerline velocity) in diffuser and tailpipe. Inlet Reynolds number, $Re_0 \approx 63.7 \times 10^6$ per meter; inlet diameter, $D_0 = 7.62$ centimeters.

Estimation of Eddy Viscosity at $x/D_0 = 3.22$

It is well known that calculations of the turbulent boundary layer require a certain amount of empirical information concerning the turbulence modeling. Upon specifying the turbulence transport, the boundary layer partial differential equations of motion can be integrated directly by numerical methods. The turbulence model of interest in this study is based on the mixing length concept in which the turbulence or eddy viscosity is related to the mean flow properties. In the boundary layer analysis of reference 1, which has been applied to the present data, the eddy viscosity in the boundary layer is described by a two-layer model. This model will be reviewed briefly because of its importance relative to the predicted boundary layer in the present diffuser.

The shear stress term appearing in the equations of motion can be expressed as the sum of a viscous and Reynolds stress contribution; namely,

$$\tau = \tau_l + \tau_t = \mu \frac{\partial U}{\partial y} - \rho \overline{uv} \quad (4)$$

where

$$-\rho \overline{uv} = \rho \epsilon \frac{\partial U}{\partial y} \quad (5)$$

The eddy viscosity ϵ is related to the Reynolds stress \overline{uv} and the mean velocity gradient $\partial U/\partial y$ as shown in equation (5).

The empirical model for the eddy viscosity appearing in the analysis of reference 1 is based on a two-layer concept. In the two-layer model, the eddy viscosity in the near wall region is expressed as

$$\epsilon = \epsilon_{in} = l^2 \left| \frac{\partial U}{\partial y} \right| \quad (6)$$

where the mixing length l is given by the VanDriest (ref. 12) expression:

$$l = Ky \left[1 - \exp\left(\frac{-y}{K_2}\right) \right] \quad (7)$$

The value of K_2 in equation (7) is given by

$$K_2 = 26 \left(\frac{\rho \nu^2}{\tau_w} \right)^{1/2} \quad (8)$$

The Clauser (ref. 11) outer region model used in the analysis of reference 1 can be expressed as

$$\epsilon = \epsilon_{\text{out}} = K_1 U_c \delta^* \quad (9)$$

The constants K and K_1 in equations (7) and (9) are

$$\left. \begin{array}{l} K = 0.41 \\ K_1 = 0.016 \end{array} \right\} \quad (10)$$

The mixing length model for the inner portion of the boundary layer depends on the wall shear stress τ_w which was not measured in the present study. Therefore a direct comparison of ϵ based on equations (6) and (7) with the values of ϵ determined from the measured velocity and Reynolds stress distributions cannot be made; however, this is not the case for the outer region of the layer. As shown in equation (9), the eddy viscosity is based on the mainstream velocity U_c and the displacement thickness δ^* , where

$$\delta^* = \int_0^{R(x)} \left[1 - \frac{U(x,y)}{U_c(x)} \right] \left[1 - \frac{y}{R(x)} \cos \sigma \right] dy \quad (11)$$

The eddy viscosity function $\epsilon/\delta^* U_c(x)$ for the outer region of the boundary layer was determined from the boundary layer measurements at $x/D_0 = 3.22$. This station was selected because it represents the only station downstream of the diffuser entrance in which the boundary layer has not completely filled the channel (refer to fig. 3). The results of $\epsilon/\delta^* U_c(x)$ are plotted as a function of $y/R(x)$ in figure 11. The standard constant K_1 ($K_1 = 0.016$) in the analysis of reference 1 is shown as a dashed line.

Although there are inaccuracies in the measured values of \overline{uv} , an eddy viscosity distribution can be presented. Clearly, the experimental distribution of K_1 in figure 11 differs from the constant value of 0.016 which was used in the Clauser outer region model (ref. 11). The Clauser model does not appear to apply to the present results be-

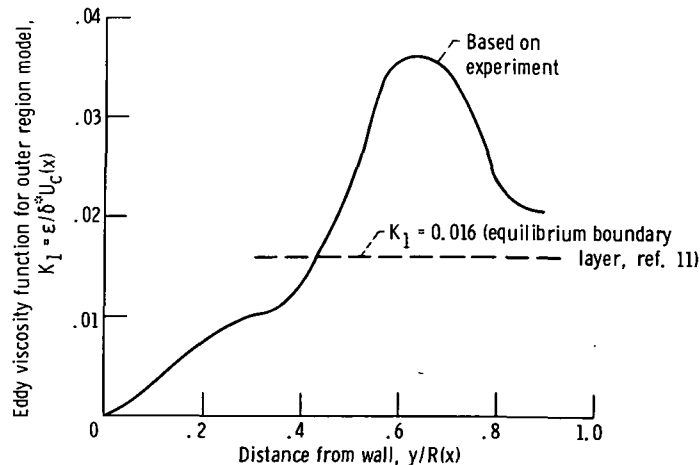


Figure 11. - Eddy viscosity distribution based on measured mean velocity and Reynolds stress distributions at axial distance $x/D_0 = 3.22$. Boundary layer displacement thickness, $\delta^* = 1.45$ centimeters; centerline velocity, $U_c(x) = 30.2$ meters per second; radius, $R(x) = 6.54$ centimeters.

cause it underestimates the outer region turbulence transport. Alternatively, in the absence of a more definitive model, the results of figure 11 suggest that the outer region constant K_1 might be increased to account for the increased turbulence. The effect of K_1 on the predicted pressure recovery coefficients and boundary layer velocity profile at $x/D_0 = 3.22$ will be presented in the following section of the report.

PREDICTED RESULTS

It is recognized that the unsteady effects associated with incipient separation are not taken into account by conventional equilibrium turbulence models. Although the neglect of the unsteady phenomena is valid for a large number of nonzero pressure gradient flows, this may not be the case for flows at incipient separation. Unfortunately these unsteady effects are not well understood and therefore in order to estimate the boundary layer in such flows it is necessary to resort to existing turbulence models. With this in mind, the sophisticated finite-difference diffuser calculational method of reference 1 has been applied to the present flow in an effort to predict the pressure recovery and mean velocity profiles.

The method of reference 1 solves for the entire flow across the duct at each streamwise station. The problems of matching solutions for the inviscid flow and boundary layer are thereby eliminated and no difficulties exist when the boundary layer merges at the diffuser centerline. This analysis assumes that the streamlines for the actual flow through the duct will not be appreciably different from the potential flow stream-

lines, and thus it is possible to make boundary layer-type approximations in a coordinate system based upon the stream function and velocity potential of the potential flow. The viscous effects are therefore treated as a perturbation upon the inviscid flow field and are governed by parabolic partial differential equations.

Experience with the program indicated that the wall curvature at the diffuser entrance caused numerical difficulties, when the calculation was initialized at station 0 (table I). In applying the analysis to the present configuration, it was convenient to initialize the calculations upstream of the entrance, that is, in the pipe section. By starting the calculation in this way the numerical problems in the entrance were avoided and the calculation provided an estimate of the real flow conditions at the diffuser entrance.

Pressure Recovery Coefficient

Entrance region. - The results of the analysis of reference 1 which are based on a reference pressure in the pipe ($x/D_0 = -2.59$), indicate a negative value of C_p up to the diffuser entrance as shown in figure 12. The difference between the experimental and theoretical values of C_p at the diffuser entrance results from the approximations used in initializing the calculation. The error in C_p resulting from the uncertainty in the inlet pressure should not exceed 0.04.

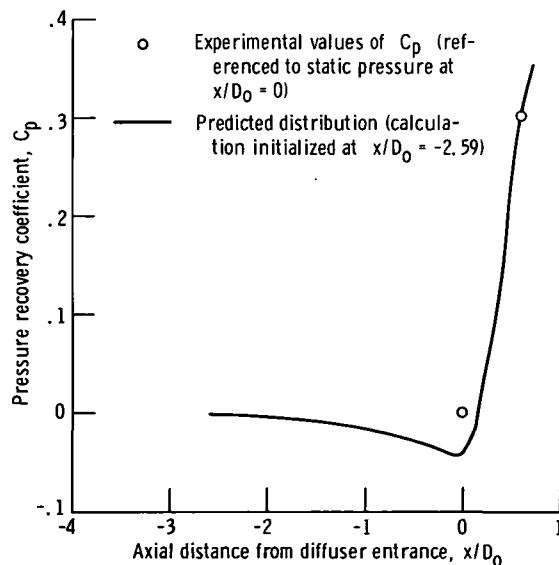


Figure 12. - Predicted pressure distribution in diffuser entrance region. Inlet Reynolds number, $Re_0 \approx 63.7 \times 10^6$ per meter; inlet diameter, $D_0 = 7.62$ centimeters.

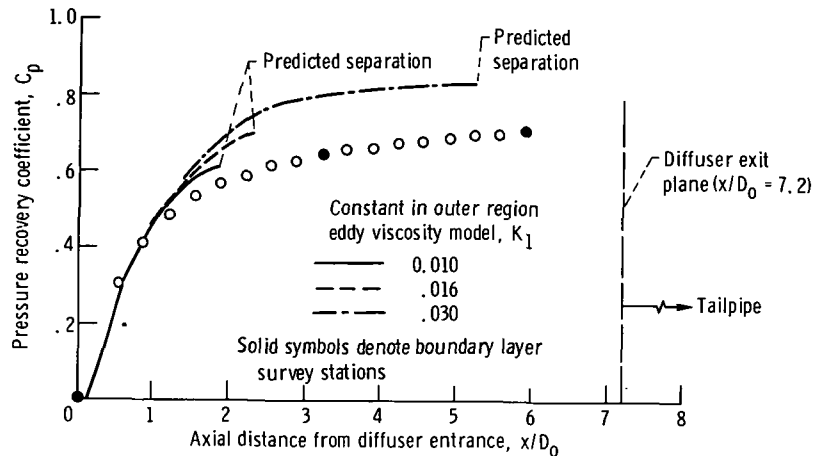


Figure 13. - Comparison of predicted and experimental pressure recovery coefficients in diffuser for various values of K_1 in outer region eddy viscosity model. Inlet Reynolds number, $Re_0 \approx 63.7 \times 10^6$ per meter; inlet diameter, $D_0 = 7.62$ centimeters.

Diffuser. - Predictions of the pressure recovery coefficient in the diffuser are compared to the experimental results in figure 13. The effect of increasing the constant K_1 in the outer region eddy viscosity model (eq. (9)) was to extend the predicted separation point further downstream and to increase the predicted values of C_p . Predicted separation occurred upstream of the survey station at $x/D_0 = 3.22$ when K_1 was equal to 0.010 and 0.016. As noted in figure 13, the calculation of C_p in the upstream portion of the diffuser was insensitive to the value of K_1 . In the early stages of diffusion the best agreement with experimental values of C_p was obtained with the low value of K_1 ($K_1 = 0.010$); however, separation was predicted very early in the expansion process. Use of the large value of K_1 ($K_1 = 0.030$) resulted in a pronounced extension of the unseparated flow region; however, the predicted values of C_p in this extended region were appreciably higher than experiment. At the predicted separation point, C_p exceeds the experimental value by about 18 percent. Although the larger value of K_1 appears more consistent with the data, the modeling of the outer eddy viscosity region exclusive of the inner region is not sufficient to accurately calculate through the nearly separated flow regime. It will be shown that estimates of C_p in this flow regime can be made with reasonable accuracy by means of the empirical constant effectiveness criterion suggested in reference 2. The results based on this simple method are influenced by the location of predicted separation. In diffusers of the present type, where incipient separation rather than actual separation occurs, the calculated separation point must be treated hypothetically since it merely delineates a region in which the turbulence modeling in the analysis breaks down. Further evidence of these deficiencies in turbulence modeling can be noted by examining the velocity profile development in the diffuser.

Velocity Profiles

The predicted velocity profiles between $x/D_0 = 0$ and 3.22 (station 9) are shown in figure 14. As indicated previously, in order to extend the calculation to $x/D_0 = 3.22$ it was necessary to use large values of K_1 ($K_1 = 0.030$). The calculated velocity profile at $x/D_0 = 3.22$ tends to attain the same general shape as the profile at incipient separation; however, the local velocities are appreciably higher than the experimental values. These higher local velocities imply a thinner boundary layer and higher C_p , consistent

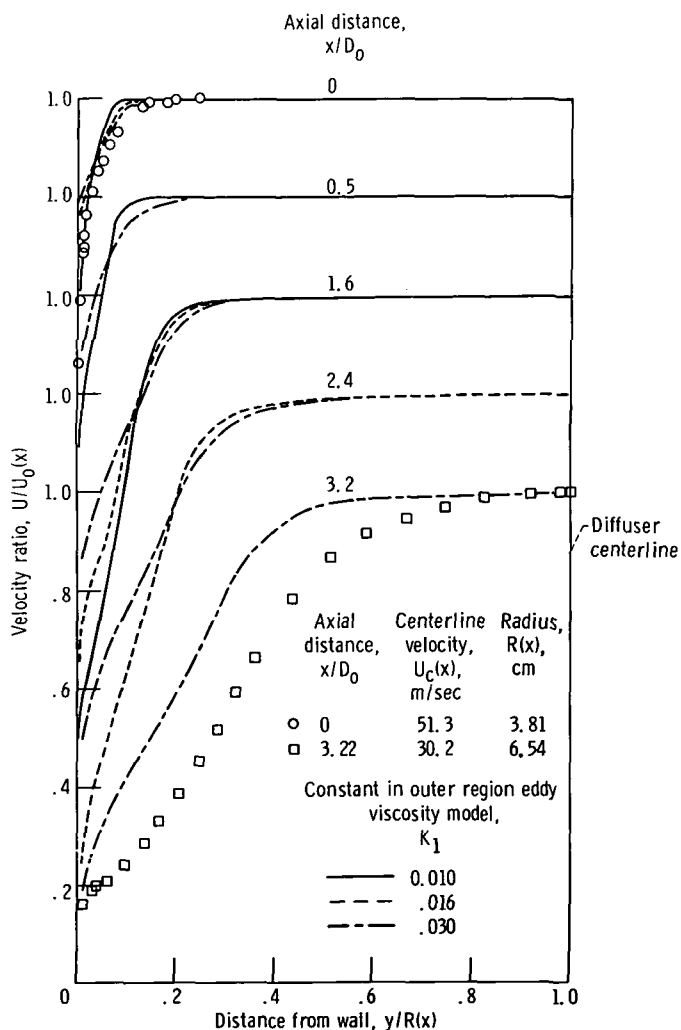


Figure 14. - Predicted boundary layer development in diffuser for different values of K_1 in outer region eddy viscosity model. Note that separation was predicted upstream of boundary layer survey at $x/D_0 = 3.2$ when $K_1 = 0.010$ and 0.016 .

with the results of figure 13. The principal effect of increasing K_1 is to increase the local velocity near the wall and, consequently, delay predicted separation.

Calculation of C_p After Predicted Separation (Ref. 2)

In reference 2 it was shown that after the predicted separation point in a conical diffuser the effectiveness η remains nearly constant, where

$$\eta = \frac{C_p}{(C_{p, id})_i} \tag{12}$$

In applying this result to the present data it was necessary to determine $\eta_{sep} = \text{constant}$ and simply multiply this constant by the ideal pressure recovery coefficient $(C_{p, id})_i$.

The results from this method are given in figure 15. The best agreement was obtained when separation was predicted at $x/D_0 = 1.8$ corresponding to the calculation with $K_1 = 0.010$. In this case the agreement was within about 12 percent of the experimental values of C_p . The largest discrepancy occurred at $x/D_0 \approx 5$ which is near the diffuser exit. Predicted results for $K_1 = 0.016$ and 0.030 are about 6 percent higher than the predictions based on $K_1 = 0.010$, or within about 18 percent of the experimental values of C_p .

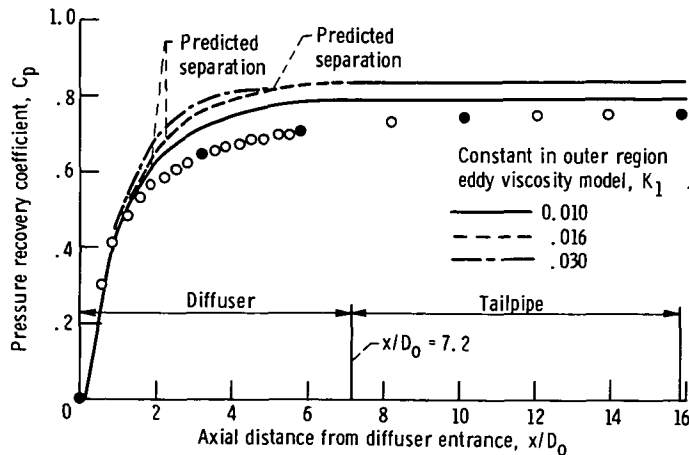


Figure 15. - Predicted pressure recovery coefficients after separation based on the constant effectiveness method (ref. 2). $Re_0 \approx 63.7 \times 10^6/m$; $D_0 = 7.62$ centimeters. Shaded symbols denote boundary layer survey stations.

COMPARISON OF TURBULENCE TRANSPORT IN ZERO PRESSURE

GRADIENT AND DIFFUSED BOUNDARY LAYERS

In the presentation of the results of the turbulent shear stress measurements emphasis was placed on the outer wake region of the boundary layer. It is of interest to further compare the turbulence results for the nearly separated boundary layer at station 9 ($x/D_0 = 3.22$) with the turbulence characteristics for a zero pressure gradient boundary layer. In making this comparison, the distributions of turbulence transport for the nearly separated boundary layer will be compared to the results for a zero pressure gradient boundary layer of thickness $\delta = R(x)$ using the turbulence measurements of Klebanoff (ref. 13). The results of reference 13 were used as input in the data reduction program of the present study in order to provide a consistent method of calculating the transport terms for the two boundary layers. The thickness of the boundary layer at $x/D_0 = 3.22$ is considered to be equal to the duct radius $R(x)$.

The transport terms to be considered are as follows: $-\overline{uv}/q^2$, $-\overline{uv} R(x)(\rho/\tau_w)^{3/2} [\partial U(x)/\partial y]$, $\overline{v^2} R(x)(\rho/\tau_w)^{3/2} [\partial U(x)/\partial y]$, and $-\overline{uv}/v^2$. These terms represent respectively, (1) the ratio of turbulent shear stress to the turbulent kinetic energy, (2) the production of turbulence, (3) the generation of Reynolds or shear stress, and (4) the ratio of the production of turbulence to the generation of Reynolds stress. Since the w' component of turbulence intensity and the wall shear stress τ_w were not measured, it was necessary to make certain assumptions in order to obtain these quantities. The turbulent kinetic energy is

$$\overline{q^2} = \overline{u^2} + \overline{v^2} + \overline{w^2} \quad (13)$$

where $\overline{w^2}$ is obtained from the approximation that

$$w' = \frac{(u' + v')}{2} \quad (14a)$$

or

$$\overline{w^2} = \frac{(\overline{u^2} + 2\overline{u'v'} + \overline{v^2})}{4} \quad (14b)$$

This assumption is quite good for the turbulent boundary layer in a zero pressure gradient (see ref. 13) and in a mild adverse pressure gradient (ref. 14). The wall shear stress was calculated for convenience from the flat plate friction law in which

$$C_f = 0.012 \operatorname{Re}_\theta^{-0.25} \quad (15)$$

and

$$\tau_w = \frac{C_f}{2} \rho U_c^2(x) \quad (16)$$

The boundary layer momentum thickness θ was given by

$$\theta = \int_0^{R(x)} \frac{U(x,y)}{U_c(x)} \left[1 - \frac{U(x,y)}{U_c(x)} \right] \left[1 - \frac{y}{R(x)} \cos \sigma \right] dy \quad (17)$$

The assumption that the shear stress can be calculated from equations (15) and (16) is questionable since the boundary layer is in a nearly separated state. In the case of complete separation C_f would be zero; however, it is obvious from equations (15) and (17) that a nonzero value of C_f would be estimated. The calculated value of τ_w in the turbulence and Reynolds stress production terms is probably too high and therefore would tend to suppress the magnitude of these terms.

The distribution of $-\overline{uv}/q^2$ is presented in figure 16. Bradshaw (ref. 15), Hinze (ref. 16), and Townsend (ref. 17) indicate that the distribution of $-\overline{uv}/q^2$ is nearly uniform over the large wake portion of the boundary layer and that $-\overline{uv}/q^2$ attains a value of about 0.14 to 0.15. These values are consistent with the calculated results using Klebanoff's data (ref. 12) for the nonaccelerated boundary layer. The greatly reduced values of $-\overline{uv}/q^2$ for the diffuser boundary layer imply that treating the viscous development in the outer portion of the boundary layer as a nonaccelerated boundary layer wake region (as in the analysis of ref. 1) may not be entirely adequate. A constant ratio of shear stress to kinetic energy also implies a similarity between the two distributions consistent with Von Kármán's similarity hypothesis concerning the structure of turbulence (ref. 16). Although the level of the distribution of $-\overline{uv}/q^2$ for the diffuser flow is much lower than the zero acceleration case, the value of $-\overline{uv}/q^2$ is approximately constant over a large portion of the diffuser boundary layer (values ranging from

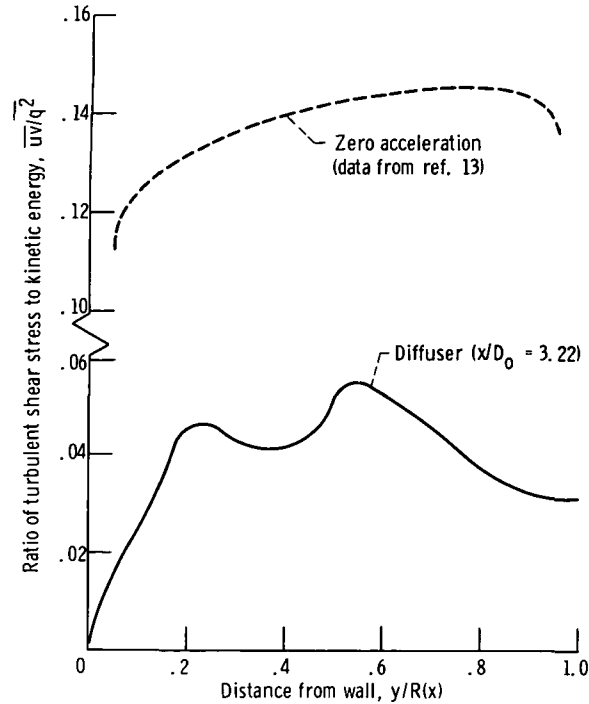


Figure 16. - Comparison of distributions of $-\overline{uv}/q^2$ for nonaccelerated and diffused boundary layers. Inlet Reynolds number, $Re_0 \approx 63.7 \times 10^6$ per meter; inlet diameter, $D_0 = 7.62$ centimeters; radius, $R(x) = 6.54$ centimeters.

about 0.04 to 0.05).

The distribution of the terms representing the production of turbulence and Reynolds stress are shown in figures 17 and 18, respectively. In the nonaccelerated boundary layer these production terms reach a peak near the wall whereas in the diffused boundary layer near separation the maximum values for the production terms occur much further from the wall ($y/R(x) \approx 0.4$). It is also apparent from figures 17 and 18 that there is a strong viscous action in the diffused boundary layer which results in the production of turbulent shear over an appreciable extent of the channel.

The ratio of the distributions of figures 17 and 18, $-\overline{uv}/v^2$, is plotted in figure 19. Note that any ambiguity in the production terms resulting primarily from the uncertainty in τ_w has been removed in forming the ratio of $-\overline{uv}/v^2$. In the nonaccelerated boundary layer the ratio of turbulence to Reynolds stress production is nearly constant over a large portion of the boundary layer; however, in the diffused boundary layer a distinct maximum occurs at $y/R(x) \approx 0.2$. In general, the ratio of $-\overline{uv}/v^2$ is lower in the diffused boundary layer, especially in the outer portion of the layer.

Examination of figures 16 and 19 reveals that there is a significant change in the

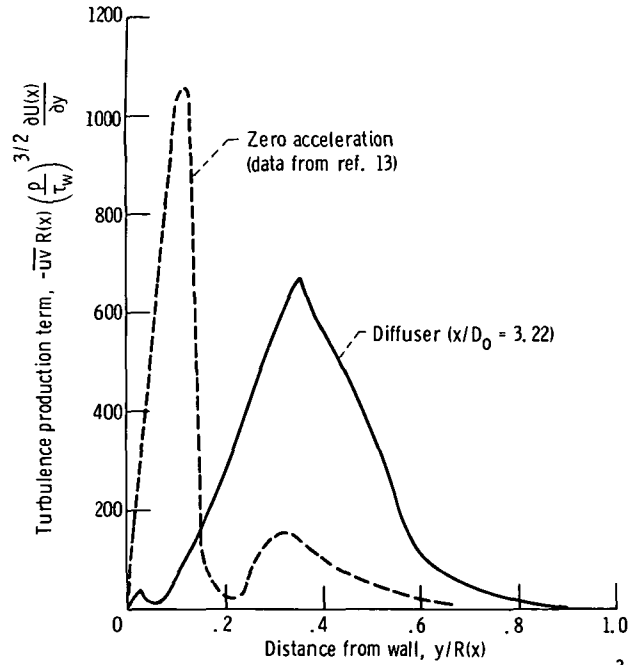


Figure 17. - Comparison of distributions of $-\bar{u}\bar{v} R(x) \left(\frac{\rho}{\tau_w}\right)^{3/2} \frac{\partial U(x)}{\partial y}$ for nonaccelerated and diffused boundary layers. Inlet Reynolds number, $Re_0 \approx 63.7 \times 10^6$ per meter; inlet diameter, $D_0 = 7.62$ centimeters; radius, $R(x) = 6.54$ centimeters.

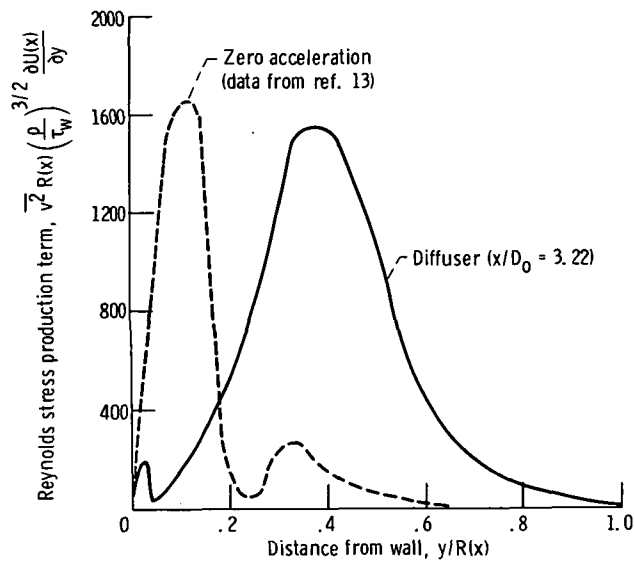


Figure 18. - Comparison of distributions of $\bar{v}^2 R(x) \left(\frac{\rho}{\tau_w}\right)^{3/2} \frac{\partial U(x)}{\partial y}$ for nonaccelerated and diffused boundary layers. Inlet Reynolds number, $Re_0 \approx 63.7 \times 10^6$ per meter; inlet diameter, $D_0 = 7.62$ centimeters; radius, $R(x) = 6.54$ centimeters.

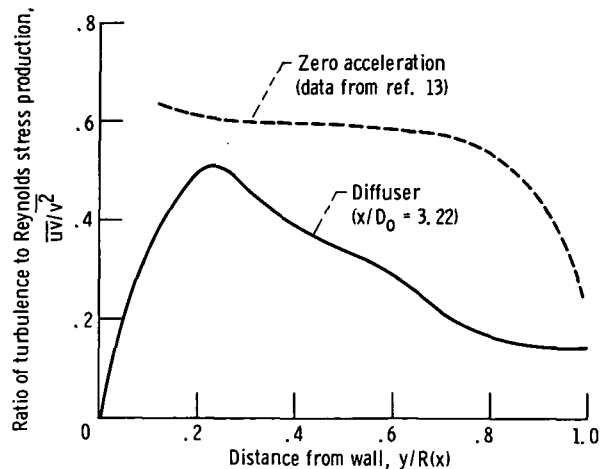


Figure 19. - Comparison of distributions of \overline{uv}/v^2 for nonaccelerated and diffused boundary layers. Inlet Reynolds number, $Re_0 \approx 63.7 \times 10^6$ per meter; inlet diameter, $D_0 = 7.62$ centimeters; radius, $R(x) = 6.54$ centimeters.

turbulence structure from that associated with a zero pressure gradient flow. The low values of \overline{uv}/q^2 for the adverse pressure gradient imply a relatively low turbulent shear for a given turbulence intensity level. The turbulent shear term, \overline{uv}/q^2 is only about one-third of the value for a zero pressure gradient flow (fig. 16). The transport of Reynolds stress by the mean flow depends on the generation as given by the product of the mean velocity gradient $\partial U/\partial y$ and the transverse turbulence component $\overline{v^2}$ (ref. 15). Likewise, the transport of turbulent kinetic energy by the mean flow depends on the production of turbulence as given by the product of the Reynolds stress and the mean velocity gradient. Therefore the low value of the ratio of turbulence production to shear production \overline{uv}/v^2 contributes to a lower change in turbulent energy relative to the change in Reynolds stress. The ratio of these production terms is generally from about 0.3 to 0.8 of the value for zero pressure gradient flow (fig. 19). Additional measurements would have to be made before conclusions can be drawn concerning the relative balance between the generation of turbulence and shear and the balance with dissipation, advection, and turbulent diffusion.

SUMMARY OF RESULTS

An experimental study was performed to determine some of the turbulence characteristics of the nearly separated flow in a 13° total angle of divergence conical diffuser coupled to a constant area tailpipe. The working fluid was air at a nominal pressure of

207 newtons per square centimeter and a nominal total temperature of 308 K. A critical flow nozzle at the exit of the tailpipe was used to limit the inlet velocity to about 51 meters per second (inlet unit Reynolds number of $63.7 \times 10^6/m$). The experimental boundary layer velocity profiles and pressure recovery coefficients were compared to theoretical results based on a diffuser boundary layer method which employs the mixing length concept. An empirical method called the constant effectiveness criterion was used to extend the prediction of pressure recovery downstream of the predicted separation point. The results of this study can be summarized as follows:

1. Hot-wire measurements of the velocity profiles at two stations in the diffuser indicated that the boundary layer was in a nearly separated state. This nearly separated condition persisted into the tailpipe recovery section.

2. The diffusion process was accompanied by extremely high values of longitudinal turbulence intensity with $u'/U_c(x)$ approaching 40 percent in the latter stages of diffusion. The maximum value of u'/U_o at the diffuser entrance was about 8 percent and occurred very close to the wall; however, as the flow diffused, the maximum value of $u'/U_c(x)$ moved towards the centerline.

3. The ratio of turbulent shear stress to turbulent kinetic energy \overline{uv}/q^2 was only about 30 percent of the accepted values for a boundary layer with a zero or mild adverse pressure gradient.

4. The maximum values for the turbulence production and Reynolds stress production for the nearly separated boundary layer occurred at an appreciable distance from the wall relative to the position of the maximum for a nonaccelerated boundary layer.

5. In the upstream portion of the diffuser good predictions of the pressure recovery coefficient were obtained with the diffuser boundary layer program; however, it is believed that separation was predicted prematurely. The value of the constant in the outer region eddy viscosity model was increased from the standard value of 0.016 to 0.030 to be more consistent with the observed turbulence structure. The effect of using a higher value of the constant was to extend the calculation an appreciably greater distance downstream but at the expense of pressure recovery accuracy. The resulting pressure recovery was about 18 percent higher than the experimental level at predicted separation.

6. Satisfactory estimates of the pressure recovery coefficient downstream of the predicted separation point were obtained by applying the constant effectiveness criterion. The best results were obtained when the predicted separation was the most premature. The agreement in this case was within about 12 percent of the experimental values of pressure recovery.

Lewis Research Center,
National Aeronautics and Space Administration,
Cleveland, Ohio, August 13, 1973,
501-24.

APPENDIX A

HOT-WIRE EQUATIONS

Two types of hot-wire probes were used to obtain the measurements in this study; namely, single wires normal to the flow and X-wires. The single wire probes were used to measure the mean velocity profiles and longitudinal component of turbulence intensity and the X-wires provided information from which the lateral component of turbulence intensity and Reynolds stress could be estimated. Since the derivation of the equations is presented in several publications, only the final form of the equations which were used in this study will be presented.

Each wire was calibrated at the diffuser centerline to obtain the bridge voltage \bar{E} as a function of the velocity U which were related according to the following general expression:

$$\bar{E}^2 = (a + bU^n)(T_w - T_e) \quad (A1)$$

where a , b , n , and $(T_w - T_e)$ are constants. The temperature difference $(T_w - T_e)$ was nominally 110 K and the value of n in equation (A1) was 0.5. Also during calibration a linearizer with zero velocity suppression was used to obtain an output signal which was directly proportional to U . The output signal from the linearizer was fed to an x-y recorder to obtain direct plots of the mean velocity profiles $U/U_c(x) = f[y/R(x)]$ in the diffuser.

The longitudinal component of turbulence intensity $u'/U_c(x)$ was calculated from the linearized form of the hot-wire equation

$$\frac{u'}{U_c(x)} = \frac{\sqrt{u'^2}}{U_c(x)} = \frac{2}{n} \frac{\sqrt{e^2} \bar{E}}{(\bar{E}^2 - \bar{E}_{ref}^2)} \frac{U}{U_c(x)} \quad (A2)$$

where \bar{E}_{ref} represents the bridge voltage at zero velocity and $\sqrt{e^2}$ is the root-mean-square (rms) component of bridge voltage. All rms quantities were measured with a 3-second time constant circuit.

The signals from the X-wire probe were fed to a commercial signal analyzer and correlator which contained a sum and difference network. The output signals from the correlator were used to calculate the lateral component of turbulence intensity $v'/U_c(x)$ and shear stress function $\bar{u}v/U_c^2(x)$. The expressions for these quantities as given in

reference 18 are

$$\frac{v'}{U_c(x)} = \frac{\sqrt{v^2}}{U_c(x)} = \left\{ \frac{\tan^2 \varphi}{n^2} \left[\frac{\overline{e_I^2 \overline{E_I^2}}}{(\overline{E_I^2} - \overline{E_{ref,I}^2})^2} + \frac{\overline{e_{II}^2 \overline{E_{II}^2}}}{(\overline{E_{II}^2} - \overline{E_{ref,II}^2})^2} - \frac{1}{2} \frac{\overline{E_I} \overline{E_{II}} \left[(e_I + e_{II})^2 - (e_I - e_{II})^2 \right]}{(\overline{E_I^2} - \overline{E_{ref,I}^2})(\overline{E_{II}^2} - \overline{E_{ref,II}^2})} \right] \right\}^{0.5} \frac{U}{U_c(x)} \quad (A3)$$

and

$$\frac{\overline{uv}}{U_c^2(x)} = \left\{ \frac{\tan \varphi}{n^2} \left[\frac{\overline{e_I^2 \overline{E_I^2}}}{(\overline{E_I^2} - \overline{E_{ref,I}^2})^2} - \frac{\overline{e_{II}^2 \overline{E_{II}^2}}}{(\overline{E_{II}^2} - \overline{E_{ref,II}^2})^2} \right] \right\} \left[\frac{U}{U_c(x)} \right]^2 \quad (A4)$$

The subscripts I and II in equations (A3) and (A4) refer to the two wires of the X-array and the angle φ ($\varphi = 45^\circ$) is the angle between the wires and the direction of the mean flow. A discussion of the effect of X-wire misalignment with the mean flow on the measured values of \overline{uv} is given in appendix B.

APPENDIX B

EFFECT OF X-WIRE MISALINEMENT ON MEASURED VALUES OF SHEAR STRESS AT THE DIFFUSER CENTERLINE

In an axisymmetric flow field having a boundary layer which extends to the duct centerline, the shear stress term \overline{uv} should be zero at the centerline and change sign in crossing the centerline. In the present study, the effect of X-wire misalignment with the mean flow direction in the vicinity of the diffuser centerline is believed to be the principal reason for observed nonzero values of \overline{uv} . This alignment error can occur at stations 9 and 17 in the diffuser since the X-wire probe is inserted into the stream in a direction normal to the wall. The effect of the resulting misalignment at the centerline can be estimated for these two stations by accounting for the unequal angles of the two wires with the mean flow direction. In appendix A the hot-wire equations were based on equal angles between the wires and mean flow direction. If these angles are unequal, the effective velocities sensed by the wires are given simply as the vector sum of the velocity components as shown with the aid of the following sketches:



Thus,

$$V_I = \left\{ \left[(U + u) \sin \alpha + v \cos \alpha \right]^2 + w^2 \right\}^{1/2} \quad (\text{B1})$$

and

$$V_{II} = \left\{ \left[-(U + u) \sin \beta + v \cos \beta \right]^2 + w^2 \right\}^{1/2} \quad (\text{B2})$$

where w is the fluctuating component of velocity perpendicular to u and v . In the following derivation only wire I will be considered since the equations pertinent to wire II can be obtained by the same procedure.

Equation (B1) (dropping the subscript I) can be expanded in a binomial series to give

$$V^n = (U \sin \alpha)^n \left(1 + \frac{u}{U} + \frac{v}{U} \cot \alpha\right)^n \quad (\text{B3})$$

where it is assumed that $w \ll U$. The equation for the hot wire relating the instantaneous voltage E to the effective velocity V is

$$E^2 = (a_1 + b_1 V^n)(T_w - T_e) \quad (\text{B4})$$

where $(T_w - T_e)$ is held constant. Substitution of equation (B3) into equation (B4) yields

$$E^2 = \left[a_1 + b_1 (U \sin \alpha)^n \left(1 + \frac{u}{U} + \frac{v}{U} \cot \alpha\right)^n \right] (T_w - T_e) \quad (\text{B5})$$

By analogy with equation (A1)

$$\overline{E^2} = [a_1 + b_1 (U \sin \alpha)^n] (T_w - T_e) \quad (\text{B6})$$

when $U = 0$,

$$\overline{E^2} = \overline{E}_{\text{ref}}^2 = a_1 (T_w - T_e)$$

or

$$\overline{E^2} - \overline{E}_{\text{ref}}^2 = b_1 (U \sin \alpha)^n (T_w - T_e) \quad (\text{B7})$$

If it is assumed that

$$\left(1 + \frac{u}{v} + \frac{v}{U} \cot \alpha\right)^n \approx 1 + n \left(\frac{u}{U} + \frac{v}{U} \cot \alpha\right) \quad (\text{B8})$$

substitution of equations (B8), (B7), and (B6) into equation (B5) yields

$$\frac{2e\overline{E}}{n(\overline{E^2} - \overline{E}_{\text{ref}}^2)} = \frac{u}{U} + \frac{v}{U} \cot \alpha \quad (\text{B9})$$

Now consider wires I and II and define

$$X \equiv \frac{2e_I \bar{E}_I}{n(\bar{E}_I^2 - \bar{E}_{\text{ref}, I}^2)} = \frac{u}{U} + \frac{v}{U} \cot \alpha \quad (\text{B10})$$

and

$$Y \equiv \frac{2e_{II} \bar{E}_{II}}{n(\bar{E}_{II}^2 - \bar{E}_{\text{ref}, II}^2)} = \frac{u}{U} - \frac{v}{U} \cot \beta \quad (\text{B11})$$

Squaring and averaging equations (B10) and (B11) yields

$$\bar{X}^2 = \frac{4e_I^2 \bar{E}_I^2}{n^2(\bar{E}_I^2 - \bar{E}_{\text{ref}, I}^2)^2} = \frac{\bar{u}^2}{U^2} + \frac{\bar{v}^2}{U^2} \cot^2 \alpha + \frac{2\bar{u}\bar{v}}{U^2} \cot \alpha \quad (\text{B12})$$

and

$$\bar{Y}^2 = \frac{4e_{II}^2 \bar{E}_{II}^2}{n^2(\bar{E}_{II}^2 - \bar{E}_{\text{ref}, II}^2)^2} = \frac{\bar{u}^2}{U^2} + \frac{\bar{v}^2}{U^2} \cot^2 \beta - \frac{2\bar{u}\bar{v}}{U^2} \cot \beta \quad (\text{B13})$$

Equation (B13) can be subtracted from equation (B12) to give the following relation for $\bar{u}\bar{v}/U^2$:

$$\frac{\bar{u}\bar{v}}{U^2} = \frac{U^2(\bar{X}^2 - \bar{Y}^2) - \bar{v}^2(\cot^2 \alpha - \cot^2 \beta)}{2U^2(\cot \alpha + \cot \beta)} \quad (\text{B14})$$

The value of \bar{v}^2 is determined by subtracting equation (B11) from equation (B10), squaring, and averaging. Then

$$\frac{\bar{v}^2}{U^2} = \frac{\bar{X}^2 - \bar{Y}^2 - 2\bar{X}\bar{Y}}{(\cot \alpha + \cot \beta)^2} \quad (\text{B15})$$

The quantities $\overline{X^2}$ and $\overline{Y^2}$ in equations (B14) and (B15) can be expressed in terms of the measured voltages by means of equations (B12) and (B13). In order to express the product \overline{XY} in terms of measured quantities it is necessary to resort to equations (B10) and (B11). From these equations the sum $\overline{(e_I + e_{II})^2}$ and difference $\overline{(e_I - e_{II})^2}$ are formed and subtracted to give

$$\overline{XY} = \frac{\overline{(e_I + e_{II})^2} - \overline{(e_I - e_{II})^2}}{n^2 \left(\frac{\overline{E_I^2} - \overline{E_{ref,I}^2}}{\overline{E_I}} \right) \left(\frac{\overline{E_{II}^2} - \overline{E_{ref,II}^2}}{\overline{E_{II}}} \right)} \quad (B16)$$

Substitution of equations (B15) and (B16) in equation (B14) leads to the following equation for $\overline{uv}/U_c^2(x)$ in terms of the measured voltages and wire angles:

$$\begin{aligned} \frac{\overline{uv}}{U_c^2(x)} = & \left(\frac{2}{n^2(\cot \alpha + \cot \beta)} \left[\frac{\overline{e_I^2 \overline{E_I^2}}}{(\overline{E_I^2} - \overline{E_{ref,I}^2})^2} - \frac{\overline{e_{II}^2 \overline{E_{II}^2}}}{(\overline{E_{II}^2} - \overline{E_{ref,II}^2})^2} \right] \right. \\ & - \frac{2(\cot \alpha - \cot \beta)}{n^2(\cot \alpha + \cot \beta)^2} \left\{ \frac{\overline{e_I^2 \overline{E_I^2}}}{(\overline{E_I^2} - \overline{E_{ref,I}^2})^2} + \frac{\overline{e_{II}^2 \overline{E_{II}^2}}}{(\overline{E_{II}^2} - \overline{E_{ref,II}^2})^2} \right. \\ & \left. \left. - \frac{1}{2} \frac{\overline{E_I \overline{E_{II}}} \left[\overline{(e_I + e_{II})^2} - \overline{(e_I - e_{II})^2} \right]}{(\overline{E_I^2} - \overline{E_{ref,I}^2})(\overline{E_{II}^2} - \overline{E_{ref,II}^2})} \right] \right\} \left[\frac{U}{U_c(x)} \right]^2 \quad (B17) \end{aligned}$$

Note that when $\alpha = \beta$, equation (B17) reduces identically to equation (A4).

When the X-wire probe is located at the centerline of the diffuser (stations 9 and 17) wire number I forms an angle of $45.0^\circ + 6.5^\circ = 51.5^\circ$ with the mean flow direction and wire number II forms an angle of $45.0^\circ - 6.5^\circ = 38.5^\circ$ with the mean flow direction. Using the data for these stations in conjunction with equation (B17) the calculated values of $\overline{uv}/U_c^2(x)$ become +0.0006 and -0.002 for stations 9 and 17, respectively. The uncorrected values of $\overline{uv}/U_c^2(x)$ for the above stations were -0.0008 and -0.006 as shown in figure 9. In both cases the angle correction tends to drive the value of \overline{uv} towards zero as expected.

A corresponding expression for $v'/U_c(x)$ can be obtained from equation (B15) and the expressions for $\overline{X^2}$, $\overline{Y^2}$, and \overline{XY} given by equations (B12), (B13), and (B16), respectively. The equation for the lateral component of turbulence intensity becomes

$$\frac{v'}{U_c(x)} = \left(\frac{4}{n^2(\cot \alpha + \cot \beta)^2} \left\{ \frac{\overline{e_I^2} \overline{E_I^2}}{(\overline{E_I^2} - \overline{E_{ref,I}^2})^2} + \frac{\overline{e_{II}^2} \overline{E_{II}^2}}{(\overline{E_{II}^2} - \overline{E_{ref,II}^2})^2} - \frac{1}{2} \frac{\overline{E_I} \overline{E_{II}} \left[(\overline{e_I + e_{II}})^2 - (\overline{e_I - e_{II}})^2 \right]}{(\overline{E_I^2} - \overline{E_{ref,I}^2})(\overline{E_{II}^2} - \overline{E_{ref,II}^2})} \right\} \right)^{0.5} \frac{U}{U_c(x)} \quad (B18)$$

This equation is identical to equation (A3) except for the factor involving the angles. Dividing equation (B18) by equation (A3) gives the ratio of v' for unequal wire angles to the value of v' based on equal angles. This ratio is simply $2/[\tan \varphi (\cot \alpha + \cot \beta)]$. Substitution of $\varphi = 45^\circ$ (appendix A) and the previous values for α and β into this term indicates that at the centerline the corrected value of v' is only 3 percent less than the measured value.

REFERENCES

1. Anderson, O. L.: User's Manual for a Finite-Difference Calculation of Turbulent Swirling Compressible Flow in Axisymmetric Ducts with Struts. Report L911211-1, United Aircraft Research Laboratories, June 1972.
2. Means, James L.; Glance, Paul C.; and Klassen, Hugh A.: Analytical Investigation of Conical Diffusers. NASA TM X-2605, 1972.
3. Sovran, Gino; and Klomp, Edward D.: Experimentally Determined Optimum Geometries for Rectilinear Diffusers with Rectangular, Conical or Annular Cross-Section. Fluid Mechanics of Internal Flow. Gino Sovran, ed., Elsevier Publ. Co., 1967, pp. 270-319.
4. Boldman, Donald R.; Neumann, Harvey E.; and Ehlers, Robert C.: Velocity, Intermittency, and Turbulence Intensity Measurements in the Boundary Layer of an Accelerated Flow. NASA TN D-6043, 1970.
5. Boldman, D. R.; Schmidt, J. F.; and Ehlers, R. C.: Effect of Uncooled Inlet Length and Nozzle Convergence Angle on the Turbulent Boundary Layer and Heat Transfer in Conical Nozzles Operating with Air. J. Heat Transfer, vol. 89, no. 4, Nov. 1967, pp. 341-350.
6. Stevens, S. J.; and Fry, P.: Measurements of the Boundary Layer Growth in Annular Diffusers. Paper 72-86, AIAA, Jan. 1972.
7. Sandborn, V. A.; and Liu, C. Y.: On Turbulent Boundary-Layer Separation. J. Fluid Mech., vol. 32, pt. 2, May 3, 1968, pp. 293-304.
8. Little, B. H., Jr.; and Wilbur, Stafford W.: Performance and Boundary-Layer Data from 12° and 23° Conical Diffusers of Area Ratio 2.0 at Mach Numbers up to 7.5×10^6 . NACA TR 1201, 1954.
9. Spangenberg, W. G.; Rowland, W. R.; and Mease, N. E.: Measurements in a Turbulent Boundary Layer Maintained in a Nearly Separating Condition. Fluid Mechanics of Internal Flow. Gino Sovran, ed., Elsevier Publ. Co., 1967, pp. 111-151.
10. Blackwelder, Ron; and Kovasznay, Leslie S. G.: Large Scale Motion of a Turbulent Boundary Layer with a Zero and a Favorable Pressure Gradient. Rep. 2, Johns Hopkins Univ. (AROD-5413-7E, AD-712330), July 1970.
11. Clauser, Francis H.: The Turbulent Boundary Layer. Advances in Applied Mechanics, vol. IV, Academic Press, New York, (1956), pp. 1-51.
12. Van Driest, E. R.: On Turbulent Flow Near a Wall. J. of Aeronautical Sci., vol. 23, no. 11, Nov. 1956.

13. Klebanoff, P. S.: Characteristics of Turbulence in a Boundary Layer with Zero Pressure Gradient. NACA Rept. 1247, 1955. (Supersedes NACA TN 3178.)
14. Anderson, P. S.; Kays, W. M.; and Moffat, R. J.: The Turbulent Boundary Layer on a Porous Plate: An Experimental Study of the Fluid Mechanics for Adverse Free-Stream Pressure Gradients. Rep. HMT-15, Stanford University (NASA CR-127817), May 1972.
15. Bradshaw, P.; and Ferriss, D. H.: Applications of a General Method of Calculating Turbulent Shear Layers. Paper 71-WA/FE-8, ASME, Nov. 1971.
16. Hinze, J. O.: Turbulence; An Introduction to its Mechanism and Theory. McGraw-Hill Book Co., Inc., 1959.
17. Townsend, A. A.: The Structure of Turbulent Shear Flow. Cambridge University Press, 1956.
18. Anon.: Applications of the Heat Flux System in Low Temperature Gases and Liquids. Technical Bulletin No. 4, Thermo-Systems Inc., Minneapolis, Minn.



POSTMASTER : If Undeliverable (Section 158
Postal Manual) Do Not Return

"The aeronautical and space activities of the United States shall be conducted so as to contribute . . . to the expansion of human knowledge of phenomena in the atmosphere and space. The Administration shall provide for the widest practicable and appropriate dissemination of information concerning its activities and the results thereof."

—NATIONAL AERONAUTICS AND SPACE ACT OF 1958

NASA SCIENTIFIC AND TECHNICAL PUBLICATIONS

TECHNICAL REPORTS: Scientific and technical information considered important, complete, and a lasting contribution to existing knowledge.

TECHNICAL NOTES: Information less broad in scope but nevertheless of importance as a contribution to existing knowledge.

TECHNICAL MEMORANDUMS: Information receiving limited distribution because of preliminary data, security classification, or other reasons. Also includes conference proceedings with either limited or unlimited distribution.

CONTRACTOR REPORTS: Scientific and technical information generated under a NASA contract or grant and considered an important contribution to existing knowledge.

TECHNICAL TRANSLATIONS: Information published in a foreign language considered to merit NASA distribution in English.

SPECIAL PUBLICATIONS: Information derived from or of value to NASA activities. Publications include final reports of major projects, monographs, data compilations, handbooks, sourcebooks, and special bibliographies.

TECHNOLOGY UTILIZATION PUBLICATIONS: Information on technology used by NASA that may be of particular interest in commercial and other non-aerospace applications. Publications include Tech Briefs, Technology Utilization Reports and Technology Surveys.

Details on the availability of these publications may be obtained from:

SCIENTIFIC AND TECHNICAL INFORMATION OFFICE

NATIONAL AERONAUTICS AND SPACE ADMINISTRATION

Washington, D.C. 20546